First Constraints on Fuzzy Dark Matter from Lyman-α Forest Data and Hydrodynamical Simulations

Vid Iršič,[1,2,3,*] Matteo Viel,[4,5,6,†] Martin G. Haehnelt,[7] James S. Bolton,[8] and George D. Becker[7,9]
[1]University of Washington, Department of Astronomy, 3910 15th Avenue Northeast, Seattle, Washington 98195-1580, USA
[2]Institute for Advanced Study, 1 Einstein Drive, Princeton, New Jersey 08540, USA
[3]The Abdus Salam International Centre for Theoretical Physics, Strada Costiera 11, I-34151 Trieste, Italy
[4]SISSA—International School for Advanced Studies, Via Bonomea 265, 34136 Trieste, Italy
[5]INAF—Osservatorio Astronomico di Trieste, Via G.B. Tiepolo 11, I-34143 Trieste, Italy
[6]INFN—National Institute for Nuclear Physics, via Valerio 2, I-34127 Trieste, Italy
[7]Institute of Astronomy and Kavli Institute of Cosmology, Madingley Road, Cambridge CB3 0HA, United Kingdom
[8]School of Physics and Astronomy, University of Nottingham, University Park, Nottingham NG7 2RD, United Kingdom
[9]Space Telescope Science Institute, 3700 San Martin Drive, Baltimore, Maryland 21218, USA
(Received 19 March 2017; revised manuscript received 8 May 2017; published 20 July 2017)

We present constraints on the masses of extremely light bosons dubbed fuzzy dark matter (FDM) from Lyman-α forest data. Extremely light bosons with a de Broglie wavelength of $\sim$1 kpc have been suggested as dark matter candidates that may resolve some of the current small scale problems of the cold dark matter model. For the first time, we use hydrodynamical simulations to model the Lyman-α flux power spectrum in these models and compare it to the observed flux power spectrum from two different data sets: the XQ-100 and HIRES/MIKE quasar spectra samples. After marginalization over nuisance and physical parameters and with conservative assumptions for the thermal history of the intergalactic medium (IGM) that allow for jumps in the temperature of up to 5000 K, XQ-100 provides a lower limit of 7.1×10^{-22} eV, HIRES/MIKE returns a stronger limit of 14.3×10^{-22} eV, while the combination of both data sets results in a limit of 20×10^{-22} eV (2σ C.L.). The limits for the analysis of the combined data sets increases to 37.5×10^{-22} eV (2σ C.L.) when a smoother thermal history is assumed where the temperature of the IGM evolves as a power law in redshift. Light boson masses in the range $1–10 \times 10^{-22}$ eV are ruled out at high significance by our analysis, casting strong doubts that FDM helps solve the "small scale crisis" of the cold dark matter models.

DOI: 10.1103/PhysRevLett.119.031302

Introduction.—Recently, there has been growing interest in so-called fuzzy dark matter (FDM) models where the dark matter is made of ultralight bosons. Cosmological and astrophysical consequences have been comprehensively reviewed in Refs. [1–5] highlighting the particle physics motivation [6–9] for such models, as well as the importance of experimental searches [10]. A broad variety of astrophysical implications have been investigated in the literature: the halo mass function [11], the innermost structure of halos [12–14], the dynamical properties of the smallest objects [15], the linear matter power spectrum [1], the development of nonlinearities by using N-body simulations [16], the abundance of high-redshift objects [17], the overall impact of FDM on galaxy formation and the reionization history of the Universe, the intergalactic medium [4,18–21], pulsar timing and binary pulsars [22,23], and the properties of our Galactic disk [24]. The general conclusion is that, in order to have an appreciable astrophysical impact, the mass of ultralight bosons would have to lie in the range $1–10 \times 10^{-22}$ eV, and in this mass range it is indeed possible that some small scale "tensions" of cold dark matter with observations could be alleviated (see, e.g., Ref. [25] for a review of the small scale "crisis" of cold dark matter).

The intergalactic medium (IGM) [26,27] plays a unique role in constraining the (small scale) matter power spectrum since the low-density, high-redshift IGM filaments are particularly sensitive to the small scale properties of dark matter. The main observable manifestation of the IGM, the Lyman-α forest, has provided important constraints on the linear matter power spectrum, especially when combined with cosmic microwave background data [28–34]. This includes, most notably, the tightest constraints on warm dark matter (WDM) models [35–40], upper limits on neutrino masses [33,40,41], and the recent remarkable discovery of baryonic acoustic oscillations in the transmitted 3D flux [42,43]. These results, especially those at small scales, are primarily due to the fact that the observed Lyman-α forest flux power spectrum provides a tracer of matter fluctuations on small scales and at high redshifts, where these fluctuations are still in the quasilinear regime. At present, the tightest limits on the free streaming of WDM, expressed as the equivalent masses of thermal WDM relics, are in the range $m_{\rm WDM} > 2.3–5$ keV at 2σ

C.L. The values at the lower end of this range are probably overly conservative and require the assumption of thermal histories that are likely unphysical [44].

In FDM models, even though the typical de Broglie scale is rather small ($\sim$ kiloparsecs), the effect of FDM on the linear matter power spectrum is noticeable on scales larger than the smallest scales typically constrained by IGM data [1]. In the absence of fully numerical FDM simulations of the flux power spectrum, it has therefore become common practice to convert the limit on thermal relic WDM models—for which the flux power spectrum has been modeled in considerable detail—into FDM limits by comparing the linear matter power spectrum of WDM and FDM models and using the mass corresponding to $k_{1/2}$, the wave number at which the linear power spectrum departs (i.e., is suppressed) from the corresponding cold dark matter power spectrum by 50%. However, the accuracy of this rather crude mapping can only be checked by performing a full set of hydrodynamical simulations to model the effect of FDM on the properties of the IGM and the Lyman-α forest. Here, we will use such simulations to provide the first constraints on FDM models based on a full modeling of the Lyman-α flux power spectrum and comparison with two high-redshift data sets well suited to probing the small scale matter power spectrum. This will also allow us to check the accuracy of the $k_{1/2}$ mapping of thermal relic WDM constraints. Our analysis will be quite similar to the one presented in Refs. [36,45], where the flux power spectrum is modeled using a set of hydrodynamical simulations that vary astrophysical and cosmological parameters combined with a Monte Carlo Markov chain analysis in the multidimensional parameter space.

Data.—The first sample we use is the set of 100 medium resolution, high signal-to-noise quasistellar object (QSO) spectra of the XQ-100 survey [46], with emission redshifts $3.5 < z < 4.5$. A more detailed description of the data and the power spectrum measurements of the XQ-100 survey can be found in Ref. [45]. Here, we repeat the most important properties of the data and the derived flux power spectrum. The spectral resolution of the X-shooter spectrograph is 30–50 km/s, depending on wavelength. The flux power spectrum used in the analysis has been calculated for a total of 114 (k, z) data points in the ranges $z = 3$, 3.2, 3.4, 3.6, 3.8, 4, 4.2 and 19 bins in k space in the range 0.003–0.057 s/km. We further use the measurements of the flux power spectrum presented in Ref. [36], at redshift bins $z = 4.2$, 4.6, 5.0, 5.4 and in 10 k bins in the range 0.001–0.08 s/km. In this second sample, the spectral resolution of the QSO absorption spectra obtained with the MIKE and HIRES spectrographs are about 13.6 and 6.7 km/s, respectively. As in the analysis of Ref. [36], a conservative cut is imposed on the flux power spectrum obtained from the MIKE and HIRES data, and only the measurements with $k > 0.005$ km^{-1} s are used to avoid possible systematic uncertainties on large scales due to continuum fitting.

Compared to XQ-100, the HIRES/MIKE sample has the advantage of probing smaller scales and higher redshift. There is a small redshift overlap between the two samples at $z = 4.2$. Since the thermal broadening (measured in km/s) of Lyman-α forest lines is roughly constant with redshift, the presence of a cutoff in the matter power spectrum due to free streaming becomes more prominent in velocity space at high redshift due to the $H(z)/(1+z)$ scaling between the fixed comoving length scale set by the free-streaming length and the corresponding velocity scale. Moreover, the 1D power spectrum is more sensitive to the presence of a cutoff compared to the 3D power spectrum.

Simulations.—Similar to Refs. [36,45], we model the flux power spectrum using a set of hydrodynamical simulations performed with the GADGET-3 code, a modified version of the publicly available GADGET-2 code [47]. A simplified star formation criterion is applied for which gas particles above an overdensity 1000 and below $T = 10^5$ K are converted into stars (see, e.g., Ref. [48]). The reference model simulation has a box length of 20 Mpc$/h$ with 2×768^3 and (cold) dark matter particles (gravitational softening of 1 comoving kpc$/h$) in a flat Λ cold dark matter (ΛCDM) Universe with cosmological parameters $\Omega_m = 0.301$, $\Omega_b = 0.0457$, $n_s = 0.961$, $H_0 = 70.2$ km s^{-1} Mpc^{-1}, and $\sigma_8 = 0.829$, in agreement with Ref. [49]. Three different WDM models with masses $m_{\rm WDM} = 2, 3, 4$ keV have also been simulated in order to obtain WDM constraints.

We simulate five different FDM models using the transfer function provided by Ref. [1] with light axion masses $\rm m_{FDM}$ of 1, 4, 5.7, 15.7, and 30×10^{-22} eV. These values have roughly the same $k_{1/2}$ as models corresponding to thermal WDM relic masses of 1, 1.73, 2, 3, and 3.87 keV, covering the relevant range for the "small scale crisis" of cold dark matter. These models were also simulated using the axionCAMB code [3] to obtain the linear transfer function, finding negligible impact on the simulated flux power. The corresponding ΛCDM model is also simulated along with a range of IGM thermal histories and cosmological parameters. In Fig. 1 we show the linear, nonlinear, and flux power spectra at $z = 5.4$ for WDM and FDM models that have the same $k_{1/2}$: nonlinearities erase some of the information contained in the linear power spectrum. Note that the 1D flux power is much more sensitive to the cutoff. The maximum wave numbers at which the flux power spectrum is measured by HIRES/MIKE and XQ-100 are represented by the horizontal arrows.

It has been noted before (see, e.g., Ref. [50]) that, for the analysis of the Lyman-α forest, it is sufficient to use the appropriate transfer function without modeling the full quantum effects below the de Broglie wavelength of the FDM particle. This hypothesis is supported by the fact that the quantum pressure starts to dominate over gravity on

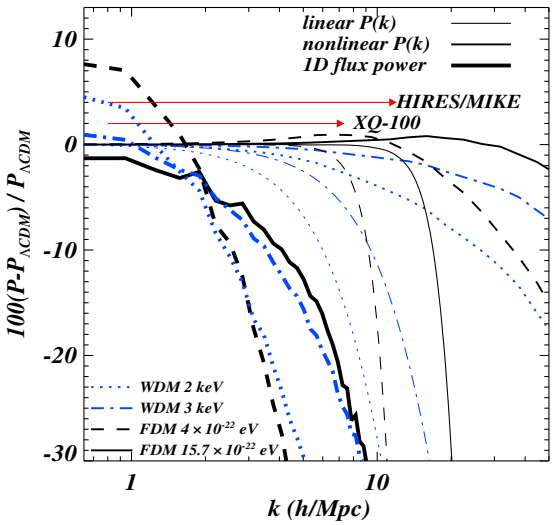

FIG. 1. Power spectrum relative to ΛCDM at $z = 5.4$ (in %). Linear matter, nonlinear matter, and flux power spectra are represented by the thin, thick, and very thick curves, respectively. Black (blue) curves are for FDM (WDM) models with $m_{\rm FDM} = 5.7, 15.7 \times 10^{-22}$ eV ($m_{\rm WDM} = 2, 3$ keV).

scales smaller than the FDM Jeans scale ($k > k_J$) [50]. The FDM Jeans scale increases with cosmic time and also with the mass of the FDM particle. For the largest redshift, $z = 5.4$, and smallest mass in our simulations, $m_{\rm FDM} = 1 \times 10^{-22}$ eV, the FDM Jeans scale is $64.7h$ Mpc^{-1}, which corresponds to scales smaller than the scale probed by our data ($k_{\rm max} = 12.7h$ Mpc^{-1} for HIRES at $z = 5.4$) [51]. The effect of the quantum pressure term should thus have a negligible effect on the structure formation relevant for the Lyman-α forest.

We vary the thermal history by modifying the photoheating rates in the simulations as in Ref. [52]. The low-density IGM ($\Delta = 1 + \delta < 10$) is well described by a power-law temperature-density relation, $T = T_0 \Delta^{\gamma - 1}$. We consider a range of values for the temperature at mean density T_0 and the slope of the $T - \rho$ relation, γ, based on the previous analysis of the Lyman-α forest and recent observations [53]. As in Ref. [45], these consist of a set of three different temperatures at mean density, $T_0(z = 3.6) = 7200, 11\,000, 14\,800$ K, which evolve with the redshift, as well as a set of three values of the slope of the $T - \rho$ relation: $\gamma(z = 3.6) = 1.0, 1.3, 1.5$. The reference thermal history assumes $(T_0(z = 3.6), \gamma(z = 3.6)) = (11\,000$ K, 1.5).

Again following Ref. [45], we use two parameters describing cosmology, σ_8 and $n_{\rm eff} = d \ln P_m(k)/d \ln k$, evaluated at $k = 0.005$ km^{-1} s. Five different values are considered for both $\sigma_8 = 0.754, 0.804, 0.829, 0.854, 0.904$ and $n_{\rm eff} = -2.3474, -2.3274, -2.3074, -2.2874, -2.2674$. The reference model has $(\sigma_8, n_{\rm eff}, n_s) = (0.829, -2.3074, 0.961)$. We also vary the redshift of reionization $z_{\rm rei}$, which is chosen to be $z_{\rm rei} = 9$ for the reference model as well as $z_{\rm rei} = 7$, 15 for two additional models [54]. The last parameter ($f_{\rm UV}$) characterizes the effect of ultraviolet (UV) background fluctuations. An extreme model dominated by QSOs has been chosen with a strong scale dependence at higher redshift and towards large scales. The mean flux is also varied *a posteriori* through rescaling the effective optical depth, $\tau_{\rm eff} = -\ln \bar{F}$. We use three different values $(0.8, 1, 1.2) \times \tau_{\rm obs,eff}$, with the observed value of $\tau_{\rm obs,eff}$ chosen to be those of the SDSS-III/BOSS measurements [57].

Method.—Using the models of the flux obtained from the simulations, we establish a grid of points for each redshift, in the parameter space of $(\bar{F}(z), T_0(z), \gamma(z), \sigma_8, z_{\rm rei}, n_{\rm eff}, f_{\rm UV}, m_{\rm FDM})$. We then perform a linear interpolation between the grid points in this multidimensional parameter space to obtain predictions of flux power for the desired models. The interpolation is performed for $P_F(k, z)$, directly, rather than for ratios of flux power with respect to the corresponding ΛCDM simulation, as was done in Ref. [36]. Parameter constraints are then obtained with a Monte Carlo Markov Chain (MCMC) code that explores the likelihood space until convergence is reached.

The redshift evolution of the IGM parameters T_0 and γ are modeled as power laws for our reference analysis: $T_0(z) = T_0^A [(1 + z)/(1 + z_p)]^{T_0^S}$ and $\gamma(z) = \gamma^A [(1 + z)/(1 + z_p)]^{\gamma^S}$. The pivot redshift is different for each data set and roughly corresponds to the redshift at which most of the data lies ($z_p = 3.6, 4.5, 4.2$ for XQ-100, HIRES/MIKE, and the combined analysis, respectively).

Results.—In Fig. 2 we show the main result of this Letter: the marginalized 1D likelihood for $1/m_{\rm FDM}$. For our reference analysis, in which the temperature evolution is parametrized as a power law at different pivot redshifts, XQ-100 returns an upper limit of 4.6×10^{-22} eV, HIRES/MIKE gives 16.4×10^{-22} eV, while the combination of the two data sets results in a considerable improvement, 37.5×10^{-22} eV (2σ C.L.). These numbers become 2.7, 16.5, 32.2×10^{-22} eV, for XQ-100, HIRES/MIKE, and both data sets, when using the following Planck priors on

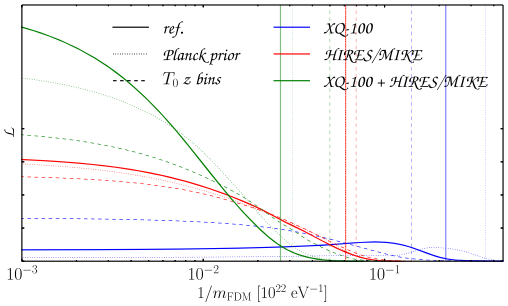

FIG. 2. 1D marginalized likelihood constraints for $1/m_{\rm FDM}$. XQ-100, HIRES/MIKE, and XQ-100+HIRES/MIKE are represented by the blue, red, and green curves, respectively, with (solid curves) and without (dotted curves) using Planck priors. Additionally, results for models where we vary temperature independently in each redshift bin are plotted as dashed curves. The 2σ upper limits are represented by vertical lines.

TABLE I. Marginalized constraints at 95% (lower limits). The pivot redshifts for different data sets are $z_p = 3.6$, 4.5, 4.2 for XQ-100, HIRES/MIKE, and a combination for the reference case, the covariance matrix multiplied by 1.3, the Planck priors, and the temperature in the redshift bins.

$m_{\rm FDM}[10^{-22}$ eV]	XQ-100	HIRES/MIKE	Combined
References	4.5	16.4	37.5
cov × 1.3	3.9	16.3	34.9
Planck priors	2.7	16.5	32.2
$T_0(z)$ bins	7.1	14.3	20.0
χ^2/d.o.f. (references)	134/124	33/40	187/173

$n_{\rm eff} = -2.307 \pm 0.01$ and $\sigma_8 = 0.829 \pm 0.01$ (1σ Gaussian priors). The improvement in the joint constraints is due to the fact that, when combining the two data sets, the thermal evolution of the IGM is assumed to be one power law for both $T_0(z)$ and $\gamma(z)$ for the full redshift range of the combined data sets. If we drop the assumption of a power-law evolution and we let the temperature vary independently in each redshift bin, with a maximum jump $\Delta T = 5000$ K in bins that are separated by $\Delta z = 0.2$, we obtain 7.1, 14.3, 20.0×10^{-22} eV for XQ-100, HIRES/MIKE, and both combined. We regard this result as the most conservative since sudden jumps of temperature are not physically plausible in this redshift range (see, e.g., Refs. [58,59]).

Increasing the covariance matrix by a multiplicative factor 1.3 in order to better represent a possible underestimation of the errors does not affect the results appreciably. In Table I we summarize the results—including the χ^2/d.o.f. for the reference case—which appear to be very reasonable in all cases. For the combined analysis, the other parameters lie within the following 2σ C.L. ranges: $z_p = 4.2$: $\sigma_8 = [0.83, 0.95]$, $n_{\rm eff} = [-2.43, -2.31]$, $T^A(z_p)[10^4\ {\rm K}] = [0.71, 1.06]$, $T^S(z_p) = [-3.37, -0.80]$, $\gamma^A(z_p) = [1.27, 1.69]$, $\gamma^S(z_p) = [-0.11, 1.82]$, $z_{\rm rei} = [6.27, 13.62]$, and $f_{\rm UV} = [0.04, 0.94]$.

We have verified the constraints obtained by considering additional simulations with an $m_{\rm FDM}$ of 30×10^{-22} eV.

In Fig. 3 we illustrate the relation between the WDM and FDM constraints. Because of the lack of detailed modeling of the flux power spectrum for FDM models using hydrodynamical simulation thus far, it has usually been assumed that one can map thermal relic WDM masses onto FDM constraints by identifying the corresponding $k_{1/2}$ values for the linear power spectra, i.e., the wave number at which the power reaches 50% of the ΛCDM linear power spectrum. Figure 3 shows that this is not a good approximation. For XQ-100 only, i.e., for a WDM constraint of 1.34 keV, the corresponding FDM limit is slightly above the $k_{1/2}$ curve, which remains a reasonable approximation. The HIRES/MIKE data only, however, give a WDM lower limit of 4.7 keV that translates into a FDM limit which is much weaker than the one that would be obtained using the $k_{1/2}$ mapping. The same holds for the combined analysis. For these higher thermal relic WDM masses, the WDM constraints are better mapped onto FDM constraints by using $k_{0.75}$ rather than $k_{1/2}$, where $k_{0.75}$ is defined as the wave number at which the power reaches 75% of the ΛCDM linear power spectrum. The reason for this is that, as the free-streaming cutoff moves to smaller scales for larger particle masses, the scales affected by the free-streaming cutoff become more nonlinear.

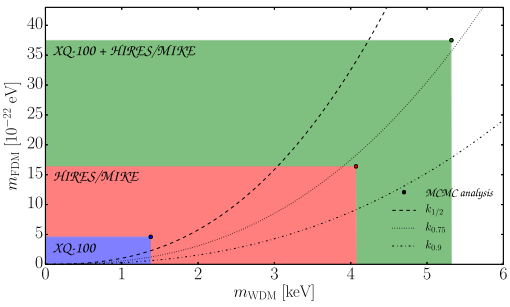

FIG. 3. Comparison of limits on $m_{\rm FDM}$ and $m_{\rm WDM}$ (thermal relic). Also shown is the relation obtained by matching $k_{1/2}$, $k_{0.75}$, and $k_{0.9}$ for the linear power spectra. Shaded areas show regions excluded by the analysis of XQ-100, HIRES/MIKE, and both data sets, in blue, red, and green, respectively. Filled circles represent the 2σ C.L. lower limits for WDM and FDM.

We have also checked to see that similar conclusions are reached when considering the 1D linear power spectrum, which is the quantity actually probed by the flux power spectrum (rather than the 3D power spectrum). The different data sets are obviously constraining linear power at different (k, z) values. Nonlinearities will develop differently in WDM and FDM models, and this makes the mapping between the two scenarios ambiguous. Full nonlinear hydrodynamic simulations and detailed modeling of the flux power spectrum is required for accurate constraints on FDM models. WDM models retain more small scale power at $k > k_{0.75}$ than the corresponding FDM model, which instead has a more prominent knee at $k < k_{0.75}$. These differences partially compensate for one another in terms of nonlinear 1D flux power in a nontrivial way that depends on how nonlinear the matter power spectrum is at the free-streaming scale. Similar to the shape of the WDM cutoff, the FDM cutoff in the flux power spectrum appears to be rather distinctive, with no significant degeneracies for the other parameters in the analysis.

Conclusions.—We have presented constraints on FDM models based on detailed modeling of the Lyman-α forest 1D flux power spectrum and high-resolution data at intermediate and high redshifts with hydrodynamical simulations. These are the first constraints that incorporate the effect of the relevant IGM physics, including thermal and pressure smoothing on the nonlinear evolution of the flux power spectrum on the relevant scales. Our final,

conservative lower limit from a joint analysis of the intermediate and high-resolution Lyman-α forest data, $m_{\rm FDM} > 20 \times 10^{-22}$ eV (2σ C.L.), was obtained with conservative assumptions for the thermal history of the IGM that allow for (unphysical) sudden jumps of the IGM temperature up to 5000 K. This lower limit for the mass of ultralight bosons strengthens by about a further factor of 2 if we assume a smoother thermal history of the IGM. Our analysis appears to close the window on FDM models with significant astrophysical implications, particularly for alleviating the tension between observations and theoretical predictions of cold dark matter models on small scales.

V. I. is supported by U.S. NSF Grant No. AST-1514734. V. I. also thanks M. McQuinn for the useful discussions and IAS, Princeton, where part of this work was completed, for its hospitality during his stay. M. V. is supported by INFN/PD51 Indark and by ERC Grant No. 257670-cosmoIGM and by PRIN-INAF 2012, "The X-shooter sample of 100 quasar spectra at $z \sim 3.5$." J. S. B. is supported by a Royal Society URF. M. G. H. is supported by the FP7 ERC Grant Emergence-320596 and the Kavli Foundation. G. D. B. is supported by the NSF under Grant No. AST-1615814. Simulations were performed at the University of Cambridge with Darwin-HPCS and COSMOS, operated on behalf of the STFC DiRAC facility (funded by BIS National E-infrastructure Capital Grant No. ST/J005673/1 and STFC Grants No. ST/H008586/1 and No. ST/K00333X/1).

Note added.—Recently, an analysis of IGM data was performed by the authors of Ref. [60], reaching conclusions similar to ours with slightly weaker constraints on the FDM mass.

*irsic@uw.edu
†viel@sissa.it

[1] W. Hu, R. Barkana, and A. Gruzinov, Fuzzy Cold Dark Matter: The Wave Properties of Ultralight Particles, Phys. Rev. Lett. **85**, 1158 (2000).
[2] T. Matos, F. S. Guzmán, and L. A. Ureña-López, Scalar field as dark matter in the Universe, Classical Quantum Gravity **17**, 1707 (2000).
[3] R. Hlozek, D. Grin, D. J. E. Marsh, and P. G. Ferreira, A search for ultralight axions using precision cosmological data, Phys. Rev. D **91**, 103512 (2015).
[4] L. Hui, J. P. Ostriker, S. Tremaine, and E. Witten, Ultralight scalars as cosmological dark matter, Phys. Rev. D **95**, 043541 (2017).
[5] T. Bernal, L. M. Fernández-Hernández, T. Matos, and M. A. Rodríguez-Meza, Rotation curves of high-resolution LSB and SPARC galaxies in wave (fuzzy) and multistate (ultralight boson) scalar field dark matter, arXiv:1701.00912.
[6] M. R. Baldeschi, G. B. Gelmini, and R. Ruffini, On massive fermions and bosons in galactic halos, Phys. Lett. **122B**, 221 (1983).
[7] J. Preskill, M. B. Wise, and F. Wilczek, Cosmology of the invisible axion, Phys. Lett. **120B**, 127 (1983).
[8] P. Sikivie and Q. Yang, Bose-Einstein Condensation of Dark Matter Axions, Phys. Rev. Lett. **103**, 111301 (2009).
[9] U.-H. Zhang and T. Chiueh, Evolution of linear wave dark matter perturbations in the radiation-dominant era, arXiv:1702.07065.
[10] P. Sikivie, Experimental Tests of the "Invisible" Axion, Phys. Rev. Lett. **51**, 1415 (1983).
[11] D. J. E. Marsh and J. Silk, A model for halo formation with axion mixed dark matter, Mon. Not. R. Astron. Soc. **437**, 2652 (2014).
[12] J.-W. Lee and I.-G. Koh, Galactic halos as boson stars, Phys. Rev. D **53**, 2236 (1996).
[13] F. S. Guzmán, T. Matos, and H. B. Villegas, Scalar fields as dark matter in spiral galaxies: Comparison with experiments, Astron. Nachr. **320**, 97 (1999).
[14] J. Zhang, Y.-L. Sming Tsai, K. Cheung, and M.-C. Chu, Ultra-light axion dark matter and its impacts on dark halo structure in N-body simulation, arXiv:1611.00892.
[15] E. Calabrese and D. N. Spergel, Ultra-light dark matter in ultra-faint dwarf galaxies, Mon. Not. R. Astron. Soc. **460**, 4397 (2016).
[16] H.-Y. Schive, T. Chiueh, and T. Broadhurst, Cosmic structure as the quantum interference of a coherent dark wave, Nat. Phys. **10**, 496 (2014).
[17] N. Menci, A. Merle, M. Totzauer, A. Schneider, A. Grazian, M. Castellano, and N. G. Sanchez, Fundamental physics with the Hubble Frontier Fields: Constraining dark matter models with the abundance of extremely faint and distant galaxies, Astrophys. J. **836**, 61 (2017).
[18] L. Amendola and R. Barbieri, Dark matter from an ultralight pseudo-Goldsone-boson, Phys. Lett. B **642**, 192 (2006).
[19] J. E. Kim and D. J. E. Marsh, An ultralight pseudoscalar boson, Phys. Rev. D **93**, 025027 (2016).
[20] D. J. E. Marsh, Axion cosmology, Phys. Rep. **643**, 1 (2016).
[21] A. Sarkar, S. K. Sethi, and S. Das, The effects of the small-scale behaviour of dark matter power spectrum on CMB spectral distortion, arXiv:1701.07273.
[22] D. Blas, D. Lopez Nacir, and S. Sibiryakov, Ultra-light dark matter resonates with binary pulsars, arXiv:1612.06789.
[23] A. Khmelnitsky and V. Rubakov, Pulsar timing signal from ultralight scalar dark matter, J. Cosmol. Astropart. Phys. 02 (2014) 019.
[24] N. Banik, A. J. Christopherson, P. Sikivie, and E. M. Todarello, New astrophysical bounds on ultralight axionlike particles, Phys. Rev. D **95**, 043542 (2017).
[25] D. H. Weinberg, J. S. Bullock, F. Governato, R. Kuzio de Naray, and A. H. G. Peter, Cold dark matter: Controversies on small scales, Proc. Natl. Acad. Sci. U.S.A. **112**, 12249 (2015).
[26] A. A. Meiksin, The physics of the intergalactic medium, Rev. Mod. Phys. **81**, 1405 (2009).
[27] M. McQuinn, The evolution of the intergalactic medium, Annu. Rev. Astron. Astrophys. **54**, 313 (2016).
[28] R. A. C. Croft, D. H. Weinberg, M. Bolte, S. Burles, L. Hernquist, N. Katz, D. Kirkman, and D. Tytler, Toward a

precise measurement of matter clustering: Lyα forest data at redshifts 2–4, Astrophys. J. **581**, 20 (2002).
[29] M. Zaldarriaga, R. Scoccimarro, and L. Hui, Inferring the linear power spectrum from the Lyα forest, Astrophys. J. **590**, 1 (2003).
[30] P. McDonald, Toward a measurement of the cosmological geometry at $z \sim 2$: Predicting Lyα forest correlation in three dimensions and the potential of future data sets, Astrophys. J. **585**, 34 (2003).
[31] M. Viel, M. G. Haehnelt, and V. Springel, Inferring the dark matter power spectrum from the Lyman α forest in high-resolution QSO absorption spectra, Mon. Not. R. Astron. Soc. **354**, 684 (2004).
[32] P. McDonald, U. Seljak, R. Cen, D. Shih, D. H. Weinberg, S. Burles, D. P. Schneider, D. J. Schlegel, N. A. Bahcall, J. W. Briggs, J. Brinkmann, M. Fukugita, Ž. Ivezić, S. Kent, and D. E. Vanden Berk, The linear theory power spectrum from the Lyα forest in the Sloan Digital Sky Survey, Astrophys. J. **635**, 761 (2005).
[33] U. Seljak, A. Slosar, and P. McDonald, Cosmological parameters from combining the Lyman-α forest with CMB, galaxy clustering and SN constraints, J. Cosmol. Astropart. Phys. 10 (2006) 014.
[34] A. Lidz, C.-A. Faucher-Giguère, A. Dall'Aglio, M. McQuinn, C. Fechner, M. Zaldarriaga, L. Hernquist, and S. Dutta, A measurement of small-scale structure in the 2.2–4.2 Lyα forest, Astrophys. J. **718**, 199 (2010).
[35] M. Viel, J. Lesgourgues, M. G. Haehnelt, S. Matarrese, and A. Riotto, Constraining warm dark matter candidates including sterile neutrinos and light gravitinos with WMAP and the Lyman-α forest, Phys. Rev. D **71**, 063534 (2005).
[36] M. Viel, G. D. Becker, J. S. Bolton, and M. G. Haehnelt, Warm dark matter as a solution to the small scale crisis: New constraints from high redshift Lyman-α forest data, Phys. Rev. D **88**, 043502 (2013).
[37] U. Seljak, A. Makarov, P. McDonald, and H. Trac, Can Sterile Neutrinos Be the Dark Matter?, Phys. Rev. Lett. **97**, 191303 (2006).
[38] J. Baur, N. Palanque-Delabrouille, C. Yèche, C. Magneville, and M. Viel, Lyman-alpha forests cool warm dark matter, J. Cosmol. Astropart. Phys. 08 (2016) 012.
[39] M. Viel, G. D. Becker, J. S. Bolton, M. G. Haehnelt, M. Rauch, and W. L. W. Sargent, How Cold Is Cold Dark Matter? Small-Scales Constraints from the Flux Power Spectrum of the High-Redshift Lyman-α Forest, Phys. Rev. Lett. **100**, 041304 (2008).
[40] C. Yeche, N. Palanque-Delabrouille, J. Baur, and H. du Mas des BourBoux, Constraints on neutrino masses from Lyman-alpha forest power spectrum with BOSS and XQ-100, arXiv:1702.03314.
[41] N. Palanque-Delabrouille, C. Yèche, J. Baur, C. Magneville, G. Rossi, J. Lesgourgues, A. Borde, E. Burtin, J.-M. LeGoff, J. Rich, M. Viel, and D. Weinberg, Neutrino masses and cosmology with Lyman-alpha forest power spectrum, J. Cosmol. Astropart. Phys. 11 (2015) 011.
[42] N. G. Busca *et al.*, Baryon acoustic oscillations in the Lyα forest of BOSS quasars, Astron. Astrophys. **552**, A96 (2013).
[43] A. Slosar *et al.*, Measurement of baryon acoustic oscillations in the Lyman-α forest fluctuations in BOSS Data Release 9, J. Cosmol. Astropart. Phys. 04 (2013) 026.
[44] A. Garzilli, A. Boyarsky, and O. Ruchayskiy, Cutoff in the Lyman α forest power spectrum: Warm IGM or warm dark matter?, arXiv:1510.07006.
[45] V. Iršič, M. Viel, T. A. M. Berg, V. D'Odorico, M. G. Haehnelt, S. Cristiani, G. Cupani, T.-S. Kim, S. López, S. Ellison, G. D. Becker, L. Christensen, K. D. Denney, G. Worseck, and J. S. Bolton, The Lyman α forest power spectrum from the XQ-100 Legacy Survey, Mon. Not. R. Astron. Soc. **466**, 4332 (2017).
[46] S. López *et al.*, XQ-100: A legacy survey of one hundred $z = 3.5$–4.5 quasars observed with VLT/X-shooter, Astron. Astrophys. **594**, A91 (2016).
[47] V. Springel, The cosmological simulation codeGADGET-2, Mon. Not. R. Astron. Soc. **364**, 1105 (2005); see also http://www.mpa-garching.mpg.de/gadget/.
[48] J. S. Bolton, E. Puchwein, D. Sijacki, M. G. Haehnelt, T.-S. Kim, A. Meiksin, J. A. Regan, and M. Viel, The Sherwood simulation suite: Overview and data comparisons with the Lyman α forest at redshifts $2 \leq z \leq 5$, Mon. Not. R. Astron. Soc. **464**, 897 (2017).
[49] P. A. R. Ade, N. Aghanim, M. Arnaud, M. Ashdown, J. Aumont, C. Baccigalupi, A. J. Banday, R. B. Barreiro, J. G. Bartlett *et al.* (Planck Collaboration), Planck 2015 results. XIII. Cosmological parameters, Astron. Astrophys. **594**, A13 (2016).
[50] H.-Y. Schive, T. Chiueh, T. Broadhurst, and K.-W. Huang, Contrasting galaxy formation from quantum wave dark matter, ψDM, with ΛCDM, using Planck and Hubble data, Astrophys. J. **818**, 89 (2016).
[51] Furthermore, the growth rate ratio ξ, as defined in Ref. [50], is $\xi > 0.995$ for scales $k < 12.7h$ Mpc^{-1} for the redshift range considered in this Letter. The value of ξ decreases as we approach the FDM Jeans scale, with $\xi = 0.55$ at $k = 40h$ Mpc^{-1}.
[52] J. S. Bolton, M. Viel, T.-S. Kim, M. G. Haehnelt, and R. F. Carswell, Possible evidence for an inverted temperature-density relation in the intergalactic medium from the flux distribution of the Lyα forest, Mon. Not. R. Astron. Soc. **386**, 1131 (2008).
[53] G. D. Becker, J. S. Bolton, M. G. Haehnelt, and W. L. W. Sargent, Detection of extended He II reionization in the temperature evolution of the intergalactic medium, Mon. Not. R. Astron. Soc. **410**, 1096 (2011).
[54] See Supplemental Material at http://link.aps.org/supplemental/10.1103/PhysRevLett.119.031302, which includes Refs. [55–56], for a discussion of how the temperature and the redshift of reionization affect the thermal Jeans smoothing.
[55] N. Y. Gnedin and L. Hui, Probing the Universe with the Lyman alpha forest: 1. Hydrodynamics of the low density IGM, Mon. Not. R. Astron. Soc. **296**, 44 (1998).
[56] G. Kulkarni, J. F. Hennawi, J. Oñorbe, A. Rorai, and V. Springel, Characterizing the pressure smoothing scale of the intergalactic medium, Astrophys. J. **812**, 30 (2015).
[57] N. Palanque-Delabrouille *et al.*, The one-dimensional Lyα forest power spectrum from BOSS, Astron. Astrophys. **559**, A85 (2013).

[58] E. Puchwein, J. S. Bolton, M. G. Haehnelt, P. Madau, G. D. Becker, and F. Haardt, The photoheating of the intergalactic medium in synthesis models of the UV background, Mon. Not. R. Astron. Soc. **450**, 4081 (2015).

[59] P. R. Upton Sanderbeck, A. D'Aloisio, and M. J. McQuinn, Models of the thermal evolution of the intergalactic medium after reionization, Mon. Not. R. Astron. Soc. **460**, 1885 (2016).

[60] E. Armengaud, N. Palanque-Delabrouille, C. Yèche, D. J. E. Marsh, and J. Baur, Constraining the mass of light bosonic dark matter using SDSS Lyman-α forest, arXiv:1703.09126.